

Published in final edited form as:

*J Biotechnol.* 2012 December 15; 164(2): 188–195. doi:10.1016/j.jbiotec.2012.08.008.

## Structure-Guided Engineering of *Lactococcus lactis* Alcohol Dehydrogenase LIAdhA for Improved Conversion of Isobutyraldehyde to Isobutanol

Xiang Liu<sup>a,b</sup>, Sabine Bastian<sup>a</sup>, Christopher D. Snow<sup>a,1</sup>, Eric M. Brustad<sup>a,2</sup>, Tatyana E. Saleski<sup>a</sup>, Jian-He Xu<sup>b</sup>, Peter Meinhold<sup>c</sup>, and Frances H. Arnold<sup>a,\*</sup>

<sup>a</sup>Division of Chemistry and Chemical Engineering, California Institute of Technology, Mail code 210-41, Pasadena, CA 91125, USA

<sup>b</sup>State Key Laboratory of Bioreactor Engineering, East China University of Science and Technology, Shanghai 200237, China

<sup>c</sup>Gevo, Inc., 345 Inverness Drive S., Buiding C, Suite 310, Englewood, CO 80112, USA

### Abstract

We have determined the X-ray crystal structures of the NADH-dependent alcohol dehydrogenase LIAdhA from *Lactococcus lactis* and its laboratory-evolved variant LIAdhA<sup>RE1</sup> at 1.9 Å and 2.5 Å resolution, respectively. LIAdhA<sup>RE1</sup>, which contains three amino acid mutations (Y50F, I212T, and L264V), was engineered to increase the microbial production of isobutanol (2-methylpropan-1-ol) from isobutyraldehyde (2-methylpropanal). Structural comparison of LIAdhA and LIAdhA<sup>RE1</sup> indicates that the enhanced activity on isobutyraldehyde stems from increases in the protein's active site size, hydrophobicity, and substrate access. Further structure-guided mutagenesis generated a quadruple mutant (Y50F/N110S/I212T/L264V), whose  $K_M$  for isobutyraldehyde is ~17-fold lower and catalytic efficiency ( $k_{cat}/K_M$ ) is ~160-fold higher than wild-type LIAdhA. Combining detailed structural information and directed evolution, we have achieved significant improvements in non-native alcohol dehydrogenase activity that will facilitate the production of next-generation fuels such as isobutanol from renewable resources.

### Keywords

Alcohol dehydrogenase; Crystal structure; Site-saturation mutagenesis; Directed evolution; Isobutyraldehyde; Biofuel

© 2012 Elsevier B.V. All rights reserved.

\*Corresponding author. frances@cheme.caltech.edu (Frances H. Arnold); phone: +1 626 395 4162; Fax: +1 626 568 8743.

<sup>1</sup>Current address: Chemical and Biological Engineering, Colorado State University, 1370 Campus Delivery, Fort Collins, CO 80523, USA.

<sup>2</sup>Current address: Department of Chemistry, University of North Carolina at Chapel Hill, CB3290, Chapel Hill, NC 27599

**Publisher's Disclaimer:** This is a PDF file of an unedited manuscript that has been accepted for publication. As a service to our customers we are providing this early version of the manuscript. The manuscript will undergo copyediting, typesetting, and review of the resulting proof before it is published in its final citable form. Please note that during the production process errors may be discovered which could affect the content, and all legal disclaimers that apply to the journal pertain.

### Author contributions

X.L., S.B., C.D.S., P.M. and F.H.A. were responsible for study concept and design, analysis and interpretation of data, and preparation of manuscript. X.L., S.B., E.B., C.D.S., T.S. and J-H.X. were responsible for acquisition of data.

### Conflict of interest

F.H.A. and P.M. are co-founders and shareholders of Gevo, Inc.

### Appendix A. Supplementary materials

## 1. Introduction

Alcohol dehydrogenases (ADH, EC 1.1.1.1) are oxidoreductases that catalyze the reversible oxidation of a wide range of alcohols to the corresponding aldehydes or ketones using nicotinamide adenine dinucleotides (NAD(P)H) as coenzymes. Ubiquitous in bacteria, yeast, plants, and mammals, ADHs can be divided into three classes based on size (Reid et al., 1994): short-chain ADHs (*c.a.* 250 residues), long-chain, iron-activated ADHs (*c.a.* 385 residues), and medium-chain, zinc-dependent ADHs (*c.a.* 350 residues) which also belong to the medium-chain dehydrogenase/reductase (MDR) super-family. Several MDR-ADHs have been structurally characterized, including horse liver ADH (HLADH, Eklund et al., 1976, 2008) and yeast *Saccharomyces cerevisiae* ADH (YADH, Leskovac et al., 2002). MDR-ADHs are either dimeric or tetrameric. Dimeric ADHs are usually found in plants and mammals, whereas tetrameric ADHs are mostly found in bacteria and yeast. The MDR-ADH catalytic mechanism was established through studies of HLADH (Ramaswamy et al., 1994; Agarwal et al., 2000) and supplemented by studies of related MDR-ADHs (Eklund and Ramaswamy, 2008; Bakera et al., 2009).

ADHs play important roles in numerous natural and engineered metabolic pathways. The latter includes the work of Liao and coworkers, who engineered Ehrlich and valine biosynthetic pathways to produce isobutanol, a next-generation biofuel, in *E. coli* (Atsumi et al., 2008). Liao's isobutanol pathway diverts 2-ketoisovalerate, a valine precursor, to isobutanol by over-expression of a 2-ketoisovalerate decarboxylase and an ADH. The ADH catalyzes the final step, conversion of isobutyraldehyde to isobutanol. This pathway can be used to produce isobutanol in a variety of microorganisms including *E. coli* (Atsumi et al., 2008, 2009 and 2010; Cann and Liao, 2008; Shen and Liao, 2008; Connor and Liao, 2009; Savrasova et al., 2011; Baez et al., 2011), *Corynebacterium glutamicum* (Smith et al., 2010; Blombach et al., 2011), *Bacillus subtilis* (Li et al., 2011), and *Clostridium cellulolyticum* (Higashide et al., 2011). Atsumi and coworkers reported that the NADH-dependent AdhA from *Lactococcus lactis* (LIAdhA) functions in this pathway, as does an NADPH-dependent homologue, YqhD, that is native to *E. coli* (Atsumi et al., 2010). Although the  $K_M$  of YqhD toward isobutyraldehyde is 5-fold lower than that of LIAdhA, its preference for NADPH over NADH generates an overall cofactor imbalance in the biosynthetic pathway. To relieve the cofactor imbalance and improve isobutanol production, Bastian and coworkers in this laboratory used directed evolution by sequential rounds of random mutagenesis and screening to enhance LIAdhA activity on isobutyraldehyde (Bastian et al., 2011). The resulting ADH variant, LIAdhA<sup>RE1</sup>, contained three amino acid substitutions (Y50F, I212T, and L264V) that led to a ~7-fold decrease in  $K_M$  and a ~30-fold increase in catalytic efficiency ( $k_{cat}/K_M$ ) over wild-type LIAdhA. Inclusion of LIAdhA<sup>RE1</sup> in the isobutanol biosynthetic pathway in place of wild-type LIAdhA increased anaerobic isobutanol titer from 8.4 g/L to 13.4 g/L in a 24-hour fermentation (Bastian et al., 2011).

To better understand the activity enhancements in LIAdhA<sup>RE1</sup> and to guide further mutagenesis to decrease the  $K_M$  for isobutyraldehyde, a non-native substrate of LIAdhA, we determined the crystal structures of LIAdhA and LIAdhA<sup>RE1</sup>. We have used the structures to further improve LIAdhA<sup>RE1</sup> for this pathway and provide insights into how these improvements were achieved.

## 2. Materials and methods

### 2.1 General

Strains, plasmids and primers are listed in Tables S1 and S2, Supplemental Information. Biological media were purchased from Research Products International (Mt. Prospect, IL, USA), NADH from Codexis, Inc. (Redwood City, CA, USA), aldehydes from Sigma-

Aldrich (St. Louis, MO, USA), oligonucleotides from Integrated DNA Technologies (San Diego, CA, USA), DNA polymerases, restriction enzymes, and T4 ligase from New England Biolabs (Ipswich, MA, USA). DNA sequencing was performed by Laragen (Los Angeles, CA, USA). Standard molecular biology methods were taken from Maniatis *et al.* (Sambrook *et al.*, 1989).

## 2.2 Cloning, library construction, and heterologous expression

For crystallization purposes, the genes encoding LIAdhA and variant LIAdhA<sup>RE1</sup> were cloned into pET22b(+) (EMD Chemicals Group, Darmstadt, Germany) using *NdeI* and *XhoI* restriction sites as described previously (Bastian *et al.*, 2011) and expressed in *E. coli* BL21(DE3). Plasmids pGVRE1 and pGV29C8 harboring variants LIAdhA<sup>RE1</sup> and LIAdhA<sup>29C8</sup> served as templates for site-saturation mutagenesis and random mutagenesis library construction, respectively. The libraries were constructed using primers listed in Table S2, Supplemental Information, and expressed in yeast CEN.PK2 as described previously (Bastian *et al.*, 2011). Mutant LIAdhA<sup>RE1-T212I</sup> harboring only the Y50F and L264V mutations was constructed using plasmid pGVRE1 and primers RE1\_T212I and RE1\_T212I\_rev (Table S2, Supplemental Information).

## 2.3 Kinetic assay and high-throughput screening

ADH activities were detected by monitoring NADH consumption at 340 nm for isobutyraldehyde, acetaldehyde, and coniferaldehyde, and at 365 nm for 2-furaldehyde, hydroxymethylfurfural (5-HMF), cinnamaldehyde, 4-hydroxybenzaldehyde, syringaldehyde and vanillin, as described previously (Larroy *et al.*, 2002). All variants were purified by immobilized metal affinity chromatography (IMAC) before they were assayed. High-throughput screening was conducted using yeast lysate as described previously (Bastian *et al.*, 2011).

## 2.4 Thermostability measurements

To determine the half-denaturation temperature ( $T_{50}$ ) of LIAdhA and its variants, 30-  $\mu$ L aliquots of purified enzyme were transferred into PCR tubes. Each tube was assigned a specific incubation temperature that corresponded to a slot on the block of an Eppendorf master cycler PCR machine programmed with a gradient covering a 20°C temperature range. The measurements were conducted in duplicate. The temperature range was changed, depending on the stability of the tested enzymes, in order to cover the denaturation range. The tubes were incubated in their slots for 15 min, and the reactions were then quenched on ice. Residual activity was determined with the activity assay in a total volume of 100  $\mu$ L in a plate reader (TECAN Group Ltd., Switzerland).  $T_{50}$  is defined as the temperature at which 50% of the initial activity is retained after 15 minutes incubation.

## 2.5 Protein purification, crystallization, and data collection

Wild-type LIAdhA and variants LIAdhA<sup>RE1</sup> and LIAdhA<sup>RE1-T212I</sup> were expressed from pET22b(+) in *E. coli* BL21(DE3) and purified by IMAC as described (Bastian *et al.*, 2011). For crystallization purposes, the IMAC-purified proteins were subjected to two sequential anion exchange chromatography runs over pre-equilibrated Q Sepharose™ columns (HiTrap™ Q HP, GE Healthcare, Piscataway, NJ, USA) using an AKTA FPLC system (GE Healthcare, Waukesha, WI, USA) after a buffer exchange to buffer A (25 mM Tris pH 7.4, and 10 mM MgCl<sub>2</sub>). The anion exchange purification method consisted of a 4-column volume equilibration step with buffer A, followed by sample injection and washout of unbound sample with buffer A for two column volumes. The proteins were eluted with a linear gradient from buffer A to 100% buffer B (25 mM Tris pH 7.4, 10 mM MgCl<sub>2</sub>, and 1 M NaCl) over 10 column volumes. Both enzymes eluted at 35% buffer B. Purified proteins

(>99% purity) were then subjected to a buffer exchange to TBS buffer (50 mM Tris pH 7.4 and 150 mM NaCl) and concentrated to 12 mg/mL prior to crystallization. For determination of the oligomerization state, we performed size exclusion chromatography on a Superdex™ 200 10/300 GL column (GE Healthcare) with 20 mM Tris, pH 7.0. Prior to the gel filtration, the enzyme was purified over a HisTrap column as described above followed by a concentration step using centrifugal filter units with a 30 kDa MWCO (Millipore). The column was calibrated with gel filtration standards from Bio-Rad. Droplets (0.3 µL) of concentrated protein solutions were tested against an equal volume of 480 crystallization conditions at room temperature using the sitting drop method. The first hit appeared in 30% (v/v) polyethylene glycol 400, 0.2 M calcium acetate, 0.1 M sodium acetate pH 4.5 for LIAdhA<sup>RE1</sup> and was further refined by traditional methods employing the sitting drop method in Linbro plates (Hampton Research). The final crystallization conditions were 30% (v/v) polyethylene glycol 400, 0.2 M calcium acetate, 0.1 M sodium acetate pH 4.5 for LIAdhA<sup>RE1</sup>, and 30% (v/v) polyethylene glycol 400, 0.2 M calcium acetate, 0.1 M sodium acetate pH 5.0 for LIAdhA, and both yielded crystals in two days.

Crystals were transferred into a cryoprotectant solution of mother liquor supplemented with 25% (v/v) PEG 400 prior to flash-cooling in liquid nitrogen and shipping to the Stanford Synchrotron Radiation Laboratory (SSRL). Diffraction data were collected using a Dectris Pilatus 6M detector on beamline 12-2 at SSRL at 100 K. An X-ray wavelength of 0.954 Å was used for both proteins. Diffraction datasets were integrated with *XDS* (Kabsch, 2010) and scaled using *SCALA* (Evans, 2006).

## 2.6 Molecular replacement and structural refinement

The crystal structure of LIAdhA<sup>RE1</sup> was determined by molecular replacement. First, a homology model for LIAdhA<sup>RE1</sup> from a variety of available homologous structures was generated using MODELLER (Šali et al., 1995). The program MOLREP (Vagin and Teplyakov, 1997) in CCP4 (Bailey, 1994) was then used to identify a candidate solution in which two monomers form a contiguous beta sheet via residues 280–285. However this solution was not amenable to refinement (rigid REFMAC  $R_{\text{free}} = 0.52$ ). This solution was somewhat improved ( $R_{\text{free}} = 0.39$ ) by PHENIX Autobuild (Adams et al., 2010). To proceed, we removed large portions (~40%) of the model, deleting most of the ill-fitting Rossmann domains. This truncated model retained an  $R_{\text{free}}$  of 0.4 after applying PHENIX Refine. Given this model, a subsequent Autobuild run produced an entirely different dimer interface (via residues 97–100) with an improved  $R_{\text{free}}$  of 0.34. At this point, the density map was of sufficient quality to manually rebuild missing segments of the model in Coot (Emsley and Cowtan, 2004), leading to a productive iterative cycle between manual refinement in Coot and automated refinement using PHENIX. The structure of wild-type LIAdhA was determined using the LIAdhA<sup>RE1</sup> model.

## 2.7 Structure analysis and modeling

The crystal structure of LIAdhA was superimposed with the crystal structures of variant LIAdhA<sup>RE1</sup>, *Bacillus stearothermophilus* ADH (htADH, PDB ID: 1RJW, 50% identity) (Ceccarelli et al., 2004) and *Pseudomonas aeruginosa* ADH (PaADH, PDB ID: 1LLU, 41% identity) (Levin et al., 2004) on Ca atoms using the align tool within Pymol (The PyMOL Molecular Graphics System, Version 1.2r3pre, Schrödinger, LLC). Root mean square deviation (rmsd) values were obtained by Pymol using the align tool. NADH coordinates were extracted from PaADH after superposition of PaADH with LIAdhA and were used to model NAD<sup>+</sup> into LIAdhA and LIAdhA<sup>RE1</sup>. Isobutanol was built into LIAdhA and LIAdhA<sup>RE1</sup> structures manually using trifluoroethyl alcohol from htADH as a starting model.

## 2.8 Protein Data Bank accession codes

Coordinates and structure factors have been deposited in the Protein Data Bank with accession numbers 4EEX for LIAdhA and 4EEZ for LIAdhA<sup>RE1</sup>.

## 3. Results and Discussion

### 3.1 Crystal structures of LIAdhA and variant LIAdhA<sup>RE1</sup>

We determined the crystal structures of LIAdhA and variant LIAdhA<sup>RE1</sup> to understand the basis of the activity increase in the variant and to obtain guidance for further enzyme engineering. This work provides the first structure of an ADH from *L. lactis*. The crystallographic statistics for LIAdhA and LIAdhA<sup>RE1</sup> data collection and refinement are shown in Table 1. Both crystal structures were observed in space group C222<sub>1</sub> with two molecules per asymmetric unit. Size exclusion chromatography revealed only a peak consistent with dimer formation (see Methods). The observed dimer is likely to correspond either to the two monomers found in the crystallographic asymmetric unit (~1830 Å<sup>2</sup> buried) or to a crystallographic dimer formed via beta strand pairing of the Rossmann domain (~3450 Å<sup>2</sup> buried). Most bacterial ADHs are tetrameric, and LIAdhA represents a rare dimeric bacterial ADH. The LIAdhA<sup>RE1</sup> structure was determined by molecular replacement, and the structure of wild-type LIAdhA was determined using LIAdhA<sup>RE1</sup> as a starting model. LIAdhA and LIAdhA<sup>RE1</sup> were refined to an  $R_{\text{free}}$  of 23.0% and 20.4% at a resolution of 2.2 Å and 1.9 Å, respectively.

Structural alignment of LIAdhA and LIAdhA<sup>RE1</sup> resulted in a root mean square deviation (rmsd) of 0.19 Å, indicating the absence of large-scale structural changes attributable to the mutations. We do observe structural differences between asymmetric monomers within both LIAdhA and LIAdhA<sup>RE1</sup> crystal structures. For example, the rmsd between chains A and B of LIAdhA<sup>RE1</sup> is 1.36 Å. Alignment of these structures with an NADH-bound structure of the alcohol dehydrogenase from *Pseudomonas aeruginosa* (PaADH, PDB ID: 1LLU) shows that in both cases the tertiary structure of chain A in LIAdhA and its variant closely resembles the cofactor-bound protein (rmsd = 0.81 Å). Chain B (rmsd = 1.83 Å) shows considerable differences in the cofactor-binding domain. It is known that cofactor binding in other ADHs induces conformational changes in this region (Plapp, 2010). Together, these data suggest that the LIAdhA crystal packing permits both open and closed conformations to be observed, even in the absence of the bound reductant.

The LIAdhA monomer (Fig. 1) comprises 339 residues and contains two zinc ions, a structural zinc and a catalytic zinc. The structural zinc is tetrahedrally coordinated by four cysteine residues (Cys91, Cys94, Cys97, and Cys105). In LIAdhA, coordination of the catalytic zinc is consistent with most MDR-ADHs and involves active site amino acids Cys39, His60, and Cys147. The fourth coordination site is filled by a water molecule in the substrate/cofactor-free enzyme subunit (Aulda and Bergman, 2008).

Each LIAdhA monomer contains two distinct domains: a coenzyme-binding domain, which folds into a classical  $\alpha/\beta$  Rossmann fold (residues 148–287), and a catalytic domain (residues 1–147 and 288–339). These two domains are connected by an interdomain ‘hinge’ formed by a helix (residues 148–159) and a loop (residues 285–291), and are separated by a deep cleft that houses the active site and the catalytic zinc. LIAdhA contains a conserved proton relay system composed of Thr41 and His44; this system contributes to the transfer of protons to free solvent, which serves as a driving force for catalysis (Agarwal et al., 2000; Levin et al., 2004).

To identify molecular determinants of NADH cofactor binding, we superposed the LIAdhA and the NADH-bound PaADH structures (Levin et al., 2004). From this alignment, we infer



that the cofactor interacts with LIAdhA through a number of hydrogen bonds with the protein main chain (residues Val262, Ser286, Val288, Leu264, His40, Leu175, and Gly174) as well as several amino acid side chains (residues His44, Thr41, His40, Asp195, and Arg333) (see Fig. 2). Asp195 is conserved throughout all NADH-dependent ADHs for recognition of the two NADH ribosyl hydroxyl groups. The conserved Rossmann GxGxxG motif is also observed in LIAdhA.

### 3.2 Protein engineering of LIAdhA to increase activity on isobutyraldehyde

LIAdhA catalyzes the final step, reduction of isobutyraldehyde, in the engineered biosynthesis of isobutanol (Atsumi et al., 2008 and 2010; Bastian et al., 2011). To improve isobutanol production by this novel pathway, we previously used directed evolution to enhance the catalytic efficiency of LIAdhA for isobutyraldehyde. Random mutagenesis and subsequent recombination of beneficial mutations yielded variant LIAdhA<sup>RE1</sup> with a ~7-fold decrease in  $K_M$  and ~30-fold increase in catalytic efficiency on isobutyraldehyde (Table 2, Bastian et al., 2011). Attempts to further improve activity by random mutagenesis were unsuccessful. Using the LIAdhA<sup>RE1</sup> structure, we selected four residues based on their proximity to the substrate binding pocket, Trp86, Asn110, Leu287, and Val288, for saturation mutagenesis with the gene coding for RE1 as template. Upon screening the four individual libraries to >95% coverage we identified a variant with the additional N110S mutation. This variant, LIAdhA<sup>29C8</sup>, has a ~17-fold decrease in  $K_M$  (from 12 to 0.68 mM) and a ~160-fold increase in catalytic efficiency (from 2.8 to 440 mM<sup>-1</sup>s<sup>-1</sup>) on isobutyraldehyde compared to wild-type LIAdhA (Table 2). No improved variants were isolated from the saturation mutagenesis at residues Trp86, Leu287, or Val288.

### 3.3 Structural insights into directed evolution

#### 3.3.1 Structural basis of the increased activity of LIAdhA<sup>RE1</sup> on isobutyraldehyde

—Three mutations (Y50F, I212T, and L264V) present in LIAdhA<sup>RE1</sup> are responsible for its ~30-fold higher catalytic efficiency on isobutyraldehyde. Mutation I212T is surface-exposed in the NADH-binding domain of LIAdhA<sup>RE1</sup> and distant from the active site. Because this mutation was discovered together with Y50F (Bastian et al., 2011), we constructed the variant having only the Y50F and L264V mutations, denoted LIAdhA<sup>RE1-T212I</sup>, and compared its activity to that of LIAdhA<sup>RE1</sup> (Table 2); LIAdhA<sup>RE1-T212I</sup> has a significantly lower  $k_{cat}$ . I212T thus makes an important contribution to the increased activity, despite its location >20 Å from the active site.

Mutations L264V and Y50F lie in loops that cap the active site and have a more direct role in regulating activity on isobutyraldehyde (Fig. 3A). Making use of the known structure of zinc-bound trifluoroethanol (see Methods), we modeled zinc-bound isobutanol in the active site of LIAdhA<sup>RE1</sup> using Pymol (Fig. 3A). From this model, it is apparent that the wild-type Leu264 side chain leaves little space for the bulky terminal methyl groups of isobutyraldehyde or isobutanol. We suspect that mutation to the smaller valine provides the space to accommodate the non-native aldehyde, which is larger than the native substrate, acetaldehyde. Deletion of the Tyr hydroxyl in Y50F, which packs against the side chain of Leu264 in wild-type LIAdhA, further enlarges the substrate-binding pocket to accommodate larger substrates. Analogous mutations that increase the size and hydrophobicity of the active site cavity have been found in the yeast homolog YADH-1 (Murali and Creaser, 1986; Creaser et al., 1990). Moreover, replacement of Trp54 in YADH-1 (analogous to Tyr50 in LIAdhA) with leucine was found to broaden substrate specificity (Weinhold et al., 1995). Thus we propose that improvements in isobutyraldehyde activity in LIAdhA<sup>RE1</sup> are due to its enlarged and increasingly hydrophobic binding pocket resulting from loss of the Tyr50 hydroxyl moiety and substitution of bulky Leu264 with valine (Fig. 3A, Table 3).

The entrance to the LIAdhA active site is formed by the side chains of four residues: Tyr50, Trp86, Leu264, and Leu287. In LIAdhA<sup>RE1</sup>, shortening of the leucine side chain in L264V leads to significant opening of the entrance (Fig. 3B). It has been shown that the loop 292–299 in the horse liver enzyme HLADH, which corresponds to the loop containing Leu264 in LIAdhA, undergoes conformational changes upon cofactor binding (Plapp, 2010). Similar conformational changes are expected to be important in LIAdhA, and mutations in this loop will tune substrate binding and catalysis. We observe very subtle movements of the loop carrying Phe50 versus Tyr50 (the alpha carbon moves only 0.3 Å when residues 40–60 are aligned). As shown in Fig. 3B, the overall effect is greater substrate access that leads to the ADH catalytic zinc center. Therefore, improvements in the activity of LIAdhA<sup>RE1</sup> on isobutyraldehyde can be attributed to expansion and increased hydrophobicity of the substrate-binding pocket combined with improved substrate access to the active site.

**3.3.2 Effects of N110S on isobutyraldehyde activity in LIAdhA<sup>29C8</sup>**—If Leu264 and Tyr50 form one wall of the substrate pocket, the opposing wall comprises Leu287, Val288, Trp86, and Asn110. We carried out site-saturation mutagenesis at each of these sites and found one favorable mutation, N110S. We can only speculate on the effect of this mutation since the structure of LIAdhA<sup>29C8</sup> is not available. However, it is likely that the N110S mutation perturbs the conformation of Trp86, which in turn affects the substrate binding pocket. In most bacterial ADHs the side chain of Asn110 pi-stacks with the indole ring of the highly conserved Trp86, which lies just above the catalytic zinc. The increased activity of LIAdhA<sup>29C8</sup> may be due to a subtle, or even dramatic, reorientation of the Trp86 indole ring. For example, the N110S mutation could allow the indole ring to flip, which would significantly open the substrate channel.

Site-saturation mutagenesis of residues 86 and nearby 287 and 288 yielded no improved mutants. Residues Leu287 and Val288 are located in a loop that connects the two protein sub-domains and might be involved in the closing of the active site during cofactor binding (Colonna-Cesari et al., 1986; Hayward and Kitao, 2006). The side chain of Trp86 lies in the active site cavity; it is notable that Trp86 is conserved in almost all MDR-ADHs. Studies of Trp86 in thermophilic SsADH suggest a critical role in governing substrate specificity (Pennacchio et al., 2009). We propose that the lack of improved variants in libraries targeting Trp86, Leu287, and Val288 is due to the essential roles played by these side chains.

**3.3.3 Thermostability changes during evolution**—We were also interested in the stabilities of the LIAdhA variants, as stability is considered a determinant of the capacity of a lineage to evolve (Vendruscolo et al., 1997; Kirschner and Gerhart, 1998; Bornberg-Bauer and Chan, 1999; O’Loughlin et al., 2006). We therefore measured thermostabilities in terms of  $T_{50}$ , the temperature at which 50% of the initial activity is retained after 15 minutes incubation. Decreases in (thermo)stability often accompany mutations that increase/alter protein activity during directed evolution (Shoichet et al., 1995; Tokuriki et al., 2008). The  $T_{50}$  of variant LIAdhA<sup>RE1</sup>, however, is approximately 7°C higher than that of wild-type LIAdhA (Table 2). One underlying cause for the increase in stability is likely to be the removal of solvent-exposed hydrophobic groups. The increased thermostability associated with I212T could result from a reduced propensity for protein aggregation; this mutation removes several surface-exposed hydrophobic atoms from an edge-exposed beta strand. Similarly, the L264V mutation removes an additional solvent-exposed hydrophobic methylene as well as increasing beta-sheet propensity (Muñoz and Serrano, 1994; Street and Mayo, 1999). Introduction of the N110S mutation in LIAdhA<sup>29C8</sup> reduces  $T_{50}$  back to the wild-type level (Table 2). We hypothesize that the destabilizing effect of N110S reflects changes in orientation of the active site Trp86 aromatic ring (as discussed above). LIAdhA<sup>29C8</sup> is as stable as wild-type LIAdhA, and decreased stability cannot account for

our inability to obtain further activity improvements by directed evolution (Bloom et al., 2006; Tokuriki and Tawfik, 2009).

**3.3.4 Substrate specificity changes during directed evolution**—The mutations selected during directed evolution reshape the substrate-binding pocket to favor isobutyraldehyde binding and catalysis. We suspected that changes in substrate specificity might reflect a general increase in ADH activity on larger substrates, as such substrate ‘promiscuity’ is often observed during directed evolution for activity on novel substrates (Roodveldt and Tawfik, 2005; Fasan et al., 2008). To investigate this, we tested the ADHs in the evolutionary lineage for activity against a panel of substrates and inhibitors, including acetaldehyde as well as other aldehydes that are biologically produced and inhibit cell growth during the fermentative processes of alcohol-producing microorganisms (Klinke et al., 2004). A summary of the kinetic parameters of LIAdhA, LIAdhA<sup>RE1</sup>, and LIAdhA<sup>29C8</sup> for different aldehydes is listed in Table 3. Neither the variants nor wild-type LIAdhA exhibited detectable activity on 4-hydroxybenzaldehyde, syringaldehyde, vanillin, or coniferaldehyde under standard assay conditions. Wild-type LIAdhA exhibited high activity on acetaldehyde, cinnamaldehyde, and 2-furaldehyde, with catalytic efficiencies of 94 mM<sup>-1</sup>s<sup>-1</sup>, 39 mM<sup>-1</sup>s<sup>-1</sup>, and 57 mM<sup>-1</sup>s<sup>-1</sup>, respectively, but showed low activity for isobutyraldehyde and hydroxymethylfurfural (5-HMF) (2.8 mM<sup>-1</sup>s<sup>-1</sup> and 0.88 mM<sup>-1</sup>s<sup>-1</sup>, respectively). Directed evolution from LIAdhA to LIAdhA<sup>29C8</sup> significantly decreased  $K_M$  values for 5-HMF and isobutyraldehyde: the 5-HMF  $K_M$  decreased ~38-fold, from 22 mM to 0.57 mM, and the isobutyraldehyde  $K_M$  decreased ~17-fold, from 12 mM to 0.68 mM. Although enlarging the substrate-binding pocket facilitates access to other bulky substrates similar in size to isobutyraldehyde, the increase in  $k_{cat}$  is specific for isobutyraldehyde (Table 3).

## 4. Conclusion

Two new crystal structures of ADHs from the medium-chain dehydrogenase/reductase superfamily, LIAdhA and its evolved variant LIAdhA<sup>RE1</sup>, were determined at high resolution. Using structure-guided saturation mutagenesis, we were able to further engineer LIAdhA to obtain an overall ~17-fold decrease in  $K_M$  and a ~160-fold increase in catalytic efficiency toward isobutyraldehyde. Structural analysis and substrate profiling showed that the increased activity is accompanied by enlargement and increased hydrophobicity of the substrate-binding pocket as well as widening of the channel that provides access to the active site for bulky aldehyde substrates. Structure-guided saturation mutagenesis of key binding pocket residues and screening for improved function can identify beneficial mutations, which can be accumulated in iterative rounds, by recombination, or upon simultaneous mutagenesis at multiple positions. These approaches can rapidly optimize alcohol dehydrogenases, which are important catalysts in engineered pathways for producing fuels and chemicals.

## Supplementary Material

Refer to Web version on PubMed Central for supplementary material.

## Acknowledgments

This research was sponsored by the Army Research Laboratory and was accomplished under Cooperative Agreement Number W911NF-09-2-0022. The views and conclusions contained in this document are those of the authors and should not be interpreted as representing the official policies, either expressed or implied, of the Army Research Laboratory or the U.S. Government. The U.S. Government is authorized to reproduce and distribute reprints for Government purposes notwithstanding any copyright notation herein. X.L. received support from the China Scholarship Council (CSC), E.M.B. was supported by a Ruth L. Kirschstein National Research Service



Award (1F32-GM087102) from the National Institutes of Health, and C.D.S. was supported by a research fellowship (KUS-F1-028-03) from King Abdullah University of Science and Technology (KAUST). The Molecular Observatory is supported by the Gordon and Betty Moore Foundation, the Beckman Institute and the Sanofi-Aventis Bioengineering Research Program at Caltech.

## Abbreviations

<b>ADH</b>	alcohol dehydrogenase
<b>NADH</b>	nicotinamide adenine dinucleotide
<b>LI</b>	<i>Lactococcus lactis</i>

## References

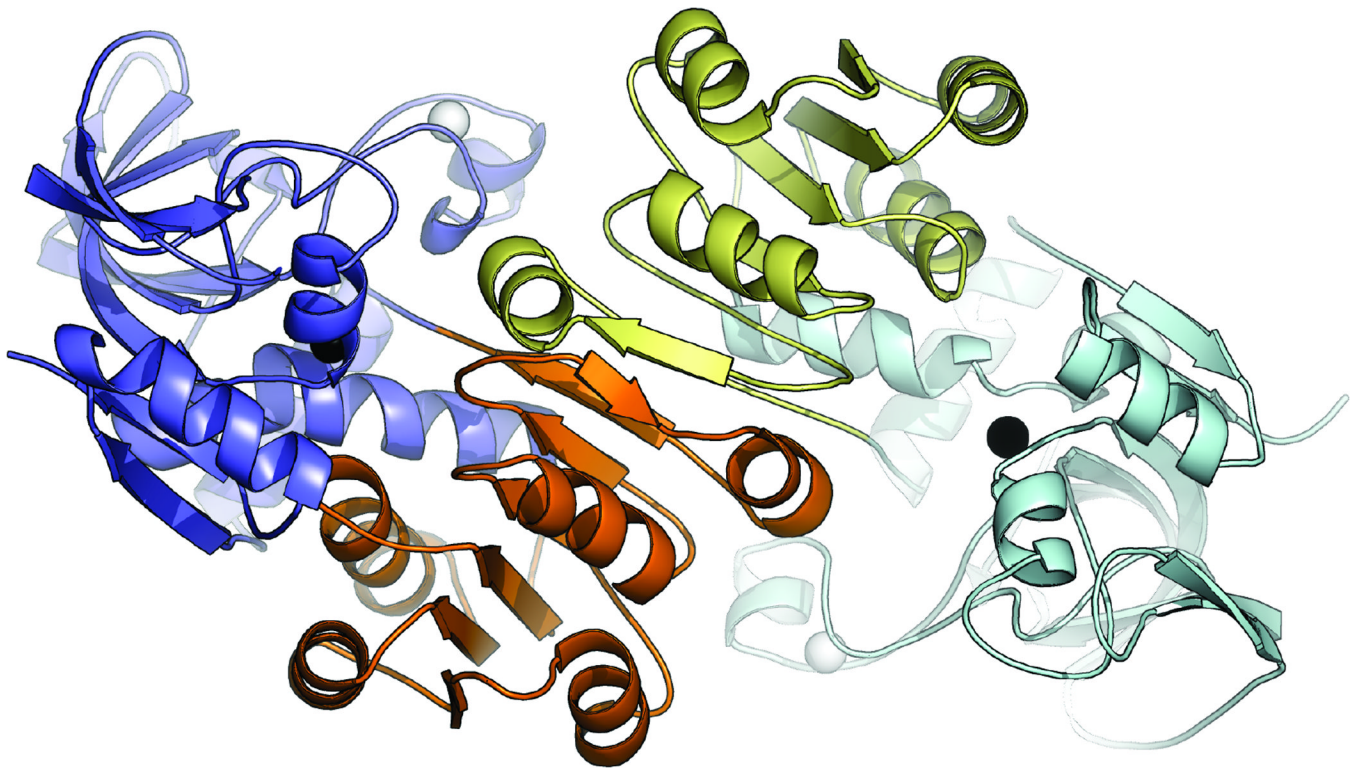
- Adams PD, Afonine PV, Bunkóczi G, Chen VB, Davis IW, Echols N, Headd JJ, Hung L-W, Kapral GJ, Grosse-Kunstleve RW, McCoy AJ, Moriarty NW, Oeffner R, Read RJ, Richardson DC, Richardson JS, Terwilliger TC, Zwart PH. *PHENIX*: a comprehensive Python-based system for macromolecular structure solution. *Acta Crystallogr. Sect. D Biol. Crystallogr.* 2010; 66:213–221. [PubMed: 20124702]
- Agarwal PK, Webb SP, Hammes-Schiffer S. Computational studies of the mechanism for proton and hydride transfer in liver alcohol dehydrogenase. *J. Am. Chem. Soc.* 2000; 122:4803–4812.
- Atsumi S, Hanai T, Liao JC. Non-fermentative pathways for synthesis of branched-chain higher alcohols as biofuels. *Nature.* 2008; 451:86–89. [PubMed: 18172501]
- Atsumi S, Li Z, Liao JC. Acetolactate synthase from *Bacillus subtilis* serves as a 2-ketoisovalerate decarboxylase for isobutanol biosynthesis in *Escherichia coli*. *Appl. Environ. Microbiol.* 2009; 75:6306–6311. [PubMed: 19684168]
- Atsumi S, Wu TY, Eckl EM, Hawkins SD, Buelter T, Liao JC. Engineering the isobutanol biosynthetic pathway in *Escherichia coli* by comparison of three aldehyde reductase/alcohol dehydrogenase genes. *Appl. Microbiol. Biotechnol.* 2010; 85:651–657. [PubMed: 19609521]
- Aulda DS, Bergman T. The role of zinc for alcohol dehydrogenase structure and function. *Cell. Mol. Life Sci.* 2008; 65:3961–3970. [PubMed: 19011745]
- Baez A, Cho KM, Liao JC. High-flux isobutanol production using engineered *Escherichia coli*: a bioreactor study with in situ product removal. *Appl. Microbiol. Biotechnol.* 2011; 90:1681–1690. [PubMed: 21547458]
- Bailey S. The *CCP4* suite: programs for protein crystallography. *Acta Crystallogr. Sect. D Biol. Crystallogr.* 1994; 50:760–763. [PubMed: 15299374]
- Bakera PJ, Brittona KL, Fishera M, Esclapezb J, Pireb C, Boneteb MJ, Ferrerb J, Ricea DW. Active site dynamics in the zinc-dependent medium chain alcohol dehydrogenase superfamily. *Proc. Natl. Acad. Sci. USA.* 2009; 106:779–784. [PubMed: 19131516]
- Bastian S, Liu X, Meyerowitz JT, Snow CD, Chen MMY, Arnold FH. Engineered ketol-acid reductoisomerase and alcohol dehydrogenase enable anaerobic 2-methylpropan-1-ol production at theoretical yield in *Escherichia coli*. *Metab. Eng.* 2011; 13:345–352. [PubMed: 21515217]
- Blombach B, Riester T, Wieschalka S, Ziert C, Youn J-W, Wendisch VF, Eikmanns BJ. *Corynebacterium glutamicum* tailored for efficient isobutanol production. *Appl. Environ. Microbiol.* 2011; 77:3300–3310. [PubMed: 21441331]
- Bloom JD, Labthavikul ST, Otey CR, Arnold FH. Protein stability promotes evolvability. *Proc. Natl. Acad. Sci. USA.* 2006; 103:5869–5874. [PubMed: 16581913]
- Bornberg-Bauer E, Chan HS. Modeling evolutionary landscapes: mutational stability, topology, and superfunnels in sequence space. *Proc. Natl. Acad. Sci. USA.* 1999; 96:10689–10694. [PubMed: 10485887]
- Cann AF, Liao JC. Production of 2-methyl-1-butanol in engineered *Escherichia coli*. *Appl. Microbiol. Biotechnol.* 2008; 81:89–98. [PubMed: 18758769]
- Ceccarelli C, Liang ZX, Strickler M, Prehna G, Goldstein BM, Klinman JP, Bahnson BJ. Crystal structure and amide H/D exchange of binary complexes of alcohol dehydrogenase from *Bacillus*

- stearothermophilus*: insight into thermostability and cofactor binding. *Biochemistry*. 2004; 43:5266–5277. [PubMed: 15122892]
- Colonna-Cesari F, Perahia D, Karplus M, Eklund H, Branden C, Tapia O. Interdomain motion in liver alcohol dehydrogenase. Structural and energetic analysis of the hinge-bending mode. *J. Biol. Chem.* 1986; 261:15273–15280. [PubMed: 3771574]
- Connor MR, Liao JC. Microbial production of advanced transportation fuels in non-natural hosts. *Curr. Opin. Biotechnol.* 2009; 20:307–315.
- Creaser EH, Murali C, Britt KA. Protein engineering of alcohol dehydrogenases; effects of amino acid changes at positions 93 and 48 of yeast ADH1. *Protein Eng.* 1990; 3:523–526. [PubMed: 2196559]
- Eklund H, Nordstrom B, Zeppezauer E, Soderlund G, Ohlsson I, Boiwe T, Soderberg B, Tapia O, Branden C, Akeson A. Three-dimensional structure of horse liver alcohol dehydrogenase at 2.4 Å resolution. *J. Mol. Biol.* 1976; 102:27–59. [PubMed: 178875]
- Eklund H, Ramaswamy S. Three-dimensional structures of MDR alcohol dehydrogenases. *Cell. Mol. Life Sci.* 2008; 65:3907–3917. [PubMed: 19011749]
- Emsley P, Cowtan K. Coot: model-building tools for molecular graphics. *Acta Crystallogr. Sect. D Biol. Crystallogr.* 2004; 60:2126–2132. [PubMed: 15572765]
- Espósito L, Sica F, Raia CA, Giordano A, Rossi M, Mazzarella L, Zagari A. Crystal structure of the alcohol dehydrogenase from the hyperthermophilic archaeon *Sulfolobus solfataricus* at 1.85 Å resolution. *J. Mol. Biol.* 2002; 318:463–477. [PubMed: 12051852]
- Evans P. Scaling and assessment of data quality. *Acta Crystallogr. Sect. D Biol. Crystallogr.* 2006; 62:72–82. [PubMed: 16369096]
- Fasan R, Meharena YT, Snow CD, Poulos TL, Arnold FH. Evolutionary history of a specialized P450 propane monooxygenase. *J. Mol. Biol.* 2008; 383:1069–1080. [PubMed: 18619466]
- Hayward S, Kitao A. Molecular dynamics simulations of NAD<sup>+</sup>-induced domain closure in horse liver alcohol dehydrogenase. *Biophys. J.* 2006; 91:1823–1831. [PubMed: 16714351]
- Higashide W, Li Y, Yang Y, Liao JC. Metabolic engineering of *Clostridium cellulolyticum* for production of isobutanol from cellulose. *Appl. Environ. Microbiol.* 2011; 77:2727–2733. [PubMed: 21378054]
- Kabsch W. *XDS* *Acta Crystallogr. Sect. D Biol. Crystallogr.* 2010; 66:125–132.
- Kirschner M, Gerhart J. Evolvability. *Proc. Natl. Acad. Sci. USA.* 1998; 95:8420–8427. [PubMed: 9671692]
- Klinke HB, Thomsen AB, Ahring BK. Inhibition of ethanol-producing yeast and bacteria by degradation products produced during pre-treatment of biomass. *Appl. Microbiol. Biotechnol.* 2004; 66:10–26. [PubMed: 15300416]
- Larroy C, Pares X, Biosca JA. Characterization of a *Saccharomyces cerevisiae* NADP(H)-dependent alcohol dehydrogenase (ADHVII), a member of the cinnamyl alcohol dehydrogenase family. *Eur. J. Biochem.* 2002; 269:5738–5745. [PubMed: 12423374]
- Leskovic V, Trivic S, Pericin D. The three zinc-containing alcohol dehydrogenases from baker's yeast, *Saccharomyces cerevisiae*. *FEMS Yeast Res.* 2002; 2:481–494. [PubMed: 12702265]
- Levin I, Meiri G, Peretz M, Burstein Y, Frolow F. The ternary complex of *Pseudomonas aeruginosa* alcohol dehydrogenase with NADH and ethylene glycol. *Protein Sci.* 2004; 13:1547–1556. [PubMed: 15152088]
- Li S, Wen J, Jia X. Engineering *Bacillus subtilis* for isobutanol production by heterologous Ehrlich pathway construction and the biosynthetic 2-ketoisovalerate precursor pathway overexpression. *Appl. Microbiol. Biotechnol.* 2011; 91:577–589. [PubMed: 21533914]
- Muñoz V, Serrano L. Intrinsic secondary structure propensities of the amino acids, using statistical  $\phi$ - $\psi$  matrices: Comparison with experimental scales. *Proteins.* 1994; 20:301–311. [PubMed: 7731949]
- Murali C, Creaser EH. Protein engineering of alcohol dehydrogenase-1. Effects of two amino acid changes in the active site of yeast ADH-1. *Protein Eng.* 1986; 1:55–57. [PubMed: 3333842]
- O'Loughlin TL, Patrick WM, Matsumura I. Natural history as a predictor of protein evolvability. *Protein Eng. Des. Sel.* 2006; 19:439–442. [PubMed: 16868005]

- Pennacchio A, Esposito L, Zagari A, Rossi M, Raia CA. Role of tryptophan 95 in substrate specificity and structural stability of *Sulfolobus solfataricus* alcohol dehydrogenase. *Extremophiles*. 2009; 13:751–761. [PubMed: 19588068]
- Plapp BV. Conformational changes and catalysis by alcohol dehydrogenase. *Arch. Biochem. Biophys.* 2010; 493:3–12. [PubMed: 19583966]
- Ramaswamy S, Eklund H, Plapp BV. Structures of horse liver alcohol dehydrogenase complexed with NAD<sup>+</sup> and substituted benzyl alcohols. *Biochemistry*. 1994; 33:5230–5237. [PubMed: 8172897]
- Ramaswamy S, Scholze M, Plapp BV. Binding of formamides to liver alcohol dehydrogenase. *Biochemistry*. 1997; 36:3522–3527. [PubMed: 9132002]
- Reid MF, Fewson CA. Molecular characterization of microbial alcohol dehydrogenases. *Crit. Rev. Microbiol.* 1994; 10:13–56. [PubMed: 8185833]
- Roodveldt C, Tawfik DS. Shared promiscuous activities and evolutionary features in various members of the amidohydrolase superfamily. *Biochemistry*. 2005; 44:12728–12736. [PubMed: 16171387]
- Šali A, Potterton L, Yuan F, van Vlijmen H, Karplus M. Evaluation of comparative protein modeling by MODELLER. *Proteins*. 1995; 23:318–326. [PubMed: 8710825]
- Sambrook, J.; Frisch, EF.; Maniatis, T. *Molecular cloning: a laboratory manual*. New York: Cold Spring Harbor Laboratory Press; 1989.
- Savrasova EA, Kivero AD, Shakulov RS, Stoyanova NV. Use of the valine biosynthetic pathway to convert glucose into isobutanol. *J. Ind. Microbiol. Biotechnol.* 2011; 38:1287–1294. [PubMed: 21161324]
- Shen CR, Liao JC. Metabolic engineering of *Escherichia coli* for 1-butanol and 1-propanol production via the keto-acid pathways. *Metab. Eng.* 2008; 10:312–320. [PubMed: 18775501]
- Shoichet BK, Baase WA, Kuroki R, Matthews BW. A relationship between protein stability and protein function. *Proc. Natl. Acad. Sci. USA*. 1995; 92:452–456. [PubMed: 7831309]
- Smith KM, Cho KM, Liao JC. Engineering *Corynebacterium glutamicum* for isobutanol production. *Appl. Microbiol. Biotechnol.* 2010; 87:1045–1055. [PubMed: 20376637]
- Street AG, Mayo SL. Intrinsic  $\beta$ -sheet propensities result from van der Waals interactions between side chains and the local backbone. *Proc. Natl. Acad. Sci. USA*. 1999; 96:9074–9076. [PubMed: 10430897]
- Tokuriki N, Stricher F, Serrano L, Tawfik DS. How protein stability and new functions trade off. *Plos Comput. Biol.* 2008; 4:e1000002. [PubMed: 18463696]
- Tokuriki N, Tawfik DS. Stability effects of mutations and protein evolvability. *Curr. Opin. Struct. Biol.* 2009; 19:596–604. [PubMed: 19765975]
- Vagin A, Teplyakov A. MOLREP: an automated program for molecular replacement. *J. Appl. Crystallogr.* 1997; 30:1022–1025.
- Vendruscolo M, Maritan A, Banavar JR. Stability threshold as a selection principle for protein design. *Phys. Rev. Lett.* 1997; 78:3967–3970.
- Weinhold EG, Benner SA. Engineering yeast alcohol dehydrogenase. Replacing Trp54 by Leu broadens substrate specificity. *Protein Eng.* 1995; 8:457–461. [PubMed: 8532667]

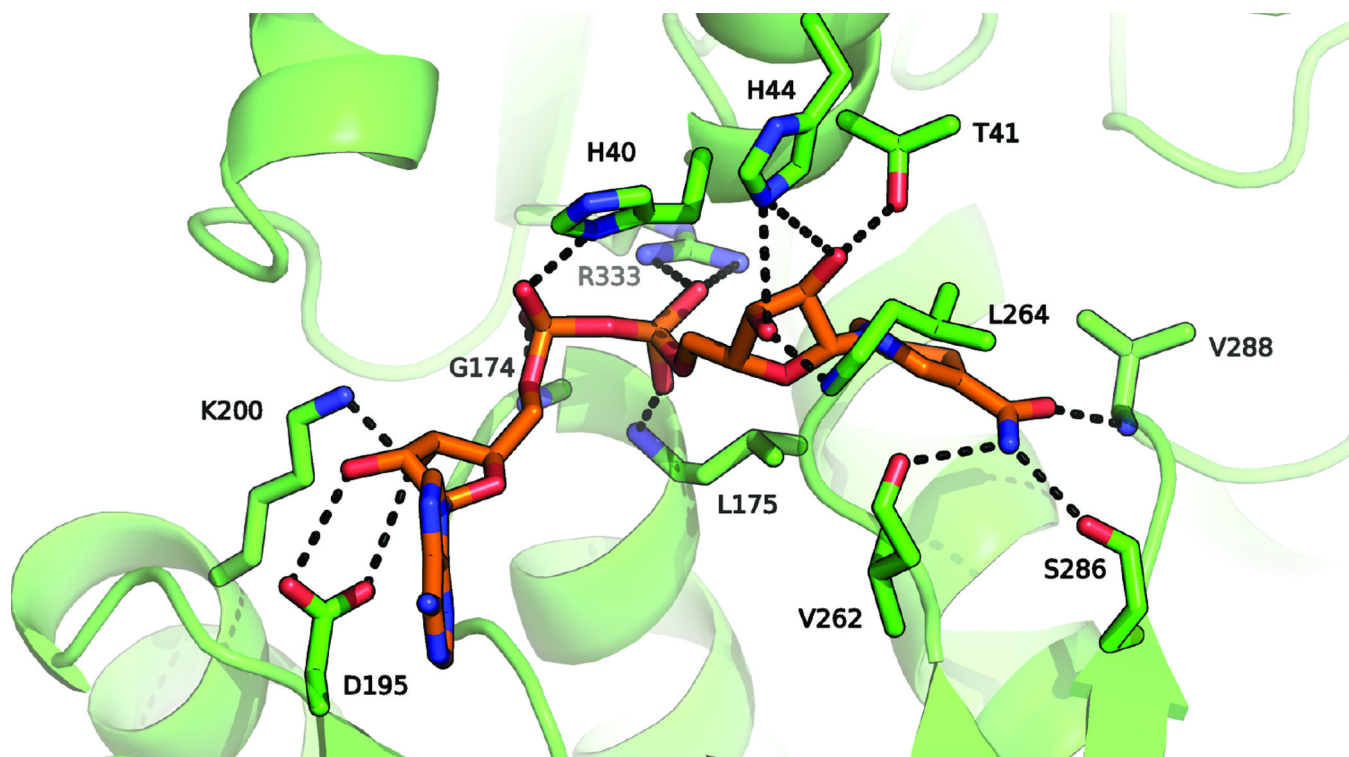
### Highlights

- The crystal structures of *L. lactis* alcohol dehydrogenase LIAdhA and its variant were determined at high resolution.
- The structure helped guide engineering of a new variant with lower  $K_M$  and higher catalytic efficiency.
- Increases in active site size, hydrophobicity, and substrate access lead to enhanced activity on isobutyraldehyde.

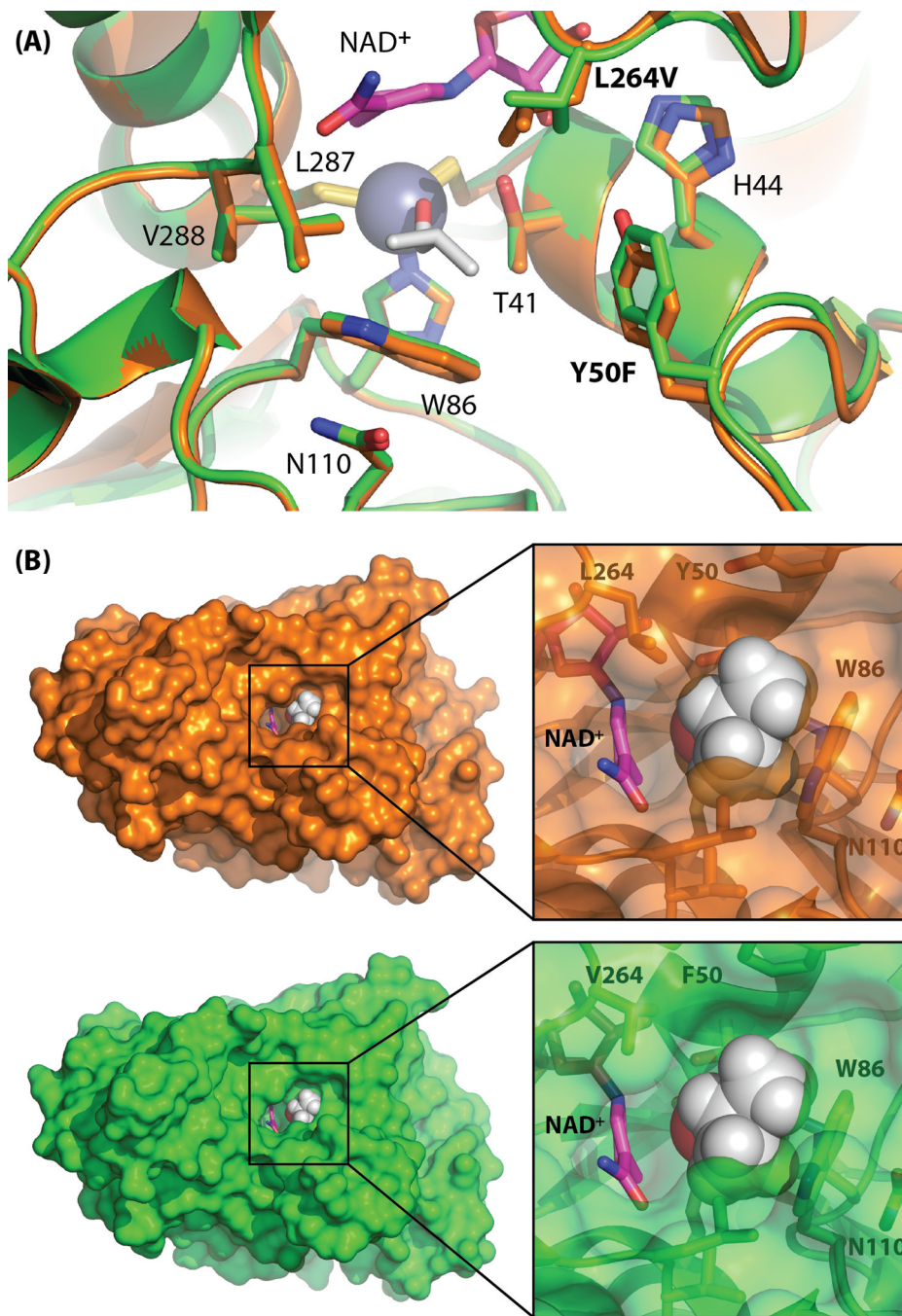


**Fig. 1.** The LIAdhA asymmetric unit dimer with catalytic domains (blue, light blue), Rossmann fold (orange, yellow), structural zinc atoms (white spheres), and catalytic zinc atoms (black spheres).





**Fig. 2.** The cofactor-binding site of LIAdhA (green), with cofactor coordinates adopted from the superimposed NADH (orange) co-crystal structure of PaADH (PDB ID: 1LLU). Hydrogen bonds to the main chain of residues Gly174, Leu175, Val262, Leu264, Ser286, and Val288 anchor NADH to the active site. The other hydroxyl groups are bound to the protein via a series of amino acids, Thr41, His40, His44 Asp195, Lys200, and Arg333.



**Fig. 3.** (A) The active site of LIAdhA (orange) superimposed with LIAdhA<sup>RE1</sup> (green). The catalytic zinc is shown as a blue sphere. Selected active site residues are shown in stick form. Thr41 and His44 are implicated in the proton conduction pathway from the active site to solvent. Isobutanol (white) and NAD<sup>+</sup> (magenta) were modeled by alignment of htADH and PaADH (see Methods), respectively. (B) Surface representation of LIAdhA (orange) and LIAdhA<sup>RE1</sup> (green) active site cavities reveals an enlarged channel opening in LIAdhA<sup>RE1</sup>'s that may result in improved access of larger non-native substrates to the active site.

**Table 1**

Crystallographic data collection and refinement statistics.

Crystal Parameters <sup>a</sup>	LIAdhA PDB ID 4EEX	LIAdhA <sup>RE1</sup> PDB ID 4EEZ
Space group	<i>C</i> 222 <sub>1</sub>	<i>C</i> 222 <sub>1</sub>
Unit cell dimensions	a=123.5 Å, b=126.5 Å, c=94.35 Å, α=β=γ=90°	a=124.4 Å, b=126.5 Å, c=94.2 Å, α=β=γ=90°
<i>Data collection statistics</i>		
Wavelength	0.954	0.954
Resolution (Å)	2.2–32.2 (2.2–2.3) <sup>b</sup>	1.9–37.8 (1.9–2.0)
Total reflections	119805	193087
Unique reflections	34501	54325
<i>R</i> <sub>merge</sub> (%)	6.4 (43.1)	5.2 (31.5)
Completeness (%)	96.6 (92.8)	97.7 (97.2)
<i>I</i> /σ <i>I</i>	11.9 (2.8)	13.8 (3.3)
<i>Refinement</i>		
<i>R</i> <sub>factor</sub> / <i>R</i> <sub>free</sub> <sup>c</sup> (%)	18.1/23.6	16.6/20.8
Protein molecules in asymmetric unit	2	2
No. of residues	680	681
No. of water molecules	188	435
No. of zinc atoms	4	4
<i>Average B-factor (Å<sup>2</sup>)</i>		
Protein	32.3	24.4
Water	32.3	30.4
<i>Geometry deviation</i>		
Rmsd on bond length (Å)	0.02	0.03
Rmsd on bond angles (deg)	1.81	1.99
<i>Ramachandran analysis (%)</i>		
Preferred regions	97.9	98.1
Outliers	0.1	0.1

<sup>a</sup> All data sets were collected from single crystals.<sup>b</sup> Highest-resolution shell is shown in parentheses.<sup>c</sup> *R*<sub>free</sub> is calculated using 5% of the reflections randomly excluded from refinement.

Kinetic parameters and thermostabilities of LIA<sub>dhA</sub> and variants, measured with isobutyraldehyde in the presence of the cofactor NADH.

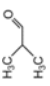



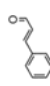
**Table 2**

Variant	Mutations	$T_{50}$ [°C]	$K_M$ [mM]	$k_{cat}$ [ $s^{-1}$ ]	$k_{cat}/K_M$ [ $mM^{-1}s^{-1}$ ]
LIA <sub>dhA</sub>	-	54.4 ± 0.4	12 ± 1	30 ± 1	2.8 ± 0.2
LIA <sub>dhA</sub> <sup>RE1-T212I</sup>	Y50F, L264V	55.2 ± 0.2	1.6 ± 0.2	50 ± 1	32 ± 4
LIA <sub>dhA</sub> <sup>RE1</sup>	Y50F, I212T, L264V	61.6 ± 0.1	1.70 ± 0.01	140 ± 1	82 ± 1
LIA <sub>dhA</sub> <sup>29C8</sup>	Y50F, N110S, I212T, L264V	55.2 ± 0.2	0.68 ± 0.07	300 ± 4	440 ± 50

All enzymes were purified prior to characterization. Errors are reported as standard deviations determined from a minimum of three independent experiments. The enzyme assays were conducted in 100 mM Tris pH 7 with 1 mM DTT, 200  $\mu$ M NADH, and 10 mM isobutyraldehyde. Concentrations of the purified enzymes were determined using the Bradford assay. The Michaelis-Menten constants for the substrate were measured with appropriate dilution series of isobutyraldehyde. Enzyme assays were performed at 25°C.

Table 3

Kinetic parameters of LIAadhA variants on related aldehydes.

Aldehydes	Structure	LIAadhA			LIAadhA <sup>RE1</sup>			LIAadhA <sup>29C8</sup>		
		$K_M$ [mM]	$k_{cat}$ [s <sup>-1</sup> ]	$k_{cat}/K_M$ [mM <sup>-1</sup> s <sup>-1</sup> ]	$K_M$ [mM]	$k_{cat}$ [s <sup>-1</sup> ]	$k_{cat}/K_M$ [mM <sup>-1</sup> s <sup>-1</sup> ]	$K_M$ [mM]	$k_{cat}$ [s <sup>-1</sup> ]	$k_{cat}/K_M$ [mM <sup>-1</sup> s <sup>-1</sup> ]
Isobutyraldehyde		12	30	2.8	1.70	140	82	0.68	300	440
Acetaldehyde		0.4	35	94	0.5	31	57	0.92	58	63
5-HMF		22	19	0.88	0.67	23	34	0.57	29	51
2-Furaldehyde		0.39	22	57	0.26	6.0	21	0.20	7	37
Cinnamaldehyde		0.7	27	39	0.24	28	140	0.16	31	210

All enzymes were purified prior to characterization. Errors are reported as standard deviations determined from a minimum of three independent experiments. The resulting standard errors are shown in Table S3, Supplemental Information. The enzyme assays were conducted in 100 mM Tris pH 7 with 1 mM DTT, 200 μM NADH, and 10 mM substrate. Concentrations of the purified enzymes were determined using the Bradford assay. The Michaelis-Menten constants for the substrate were measured with appropriate dilution series of isobutyraldehyde. Enzyme assays were performed at 25°C.